AIAA JOURNAL
Vol. 30, No. 5, May 1992

Numerical Simulation of Droplet Deformation in Convective Flows

Zheng-Tao Deng* and San-Mou Jeng†
University of Tennessee Space Institute, Tullahoma, Tennessee 37388

A computational model based on an arbitrary-Lagrangian-Eulerian numerical algorithm is developed for flows separated by a free surface where the surface tension force is important. This model is used to study deformation and oscillation of cylindrical/spherical droplets with and without external forced convection. The calculated frequency of droplet oscillation agrees well with the analytical value derived from perturbation analysis, and the amplitude of oscillation does not decay with time, which indicates that numerical diffusion and damping do not exist in the adopted algorithm. The deformation of an initially spherical droplet under forced convection is calculated and found consistent with the conclusions in the literature. Good agreement is also obtained in comparison with experimental results for an initially deformed droplet in forced convective flows.

Introduction

CURRENT spray combustion models based on finite difference solutions of the governing partial differential equations have been developed with simplified assumptions. Because the droplet spacing and droplet diameters are two to five orders of magnitude less than the cumbustor dimensions, it is not feasible to have a computational mesh sufficiently small to resolve combustor phenomena on the scale of droplet spacing or droplet diameters. With the advanced computer, it is possible to resolve only one or a few droplets at a time, but never the many thousands in a practical combustor. As a result of this, the exchange process between gas flows and droplets must be studied independently to provide a submodel for spray combustion.

During recent years, significant progress has been made in the understanding of single droplet behavior and droplet-droplet interaction within a spray combustion system. Sophisticated computational fluid dynamics (CFD) models have been used to derive the interface exchange coefficients (drag coefficient, mass transfer rate, and energy transfer rate) between a liquid propellant droplet and the surrounding hot combustion gas products. The information derived from these CFD codes for droplet behavior have been compiled and used to establish more accurate physical submodels for spray combustion in practical devices. However, most of these studies on droplet dynamics are limited to a perfect spherically shaped droplet, which essentially implies that the interfacial surface tension force is infinitely large. In reality, a droplet may experience severe aerodynamic forces during its lifetime in a combustor. For example, in practical liquid rocket combustors, the flow is turbulent, producing velocity and pressure fluctuations that interact with the liquid drops causing them to experience nonuniform accelerations. These accelerations tend to deform and break up the drops while the surface tension of the liquid tries to hold them together. The deformation affects the droplet trajectory and the surrounding flowfield, which in turn dominates the characteristics of the gas-phase combustion process. One of the conventional methods describing detailed interactions between a droplet and the external gas flowfield is to make an equivalent sphere assumption and use an empirical expression to account for interphase transport of mass, momentum, and energy. The effect due to nonspherical shape is completely neglected due to computational complexity.

The primary requirement for numerical simulation of the interaction between two immiscible fluid phases is the ability to track an arbitrarily shaped and moving material interface or discontinuity. There are two basic approaches for free surface tracking: Langrangian and Eulerian methods. A fully Lagrangian method seems to be the most natural way to track the material interface. By using a Lagrangian method, the grid moves with the same velocity as the local fluid velocity so that the interface is always located on well-defined cell boundaries. But the use of the Lagrangian method in numerical simulations has generally been restricted to well-behaved flows.[1] It is necessary to use a regriding technique to maintain acceptable numerical accuracy when severe grid distortion occurs.

A two-dimensional Lagrangian model has been developed by Fritts et al.[2] and Fyfe et al.[3,4] to simulate the two-dimensional incompressible droplet deformation under different conditions. A triangular grid system has been used in order to track the interface more accurately. But extension to three-dimensional flows introduces new complications in reconnection algorithms. Also significant bookkeeping and computer storage are required. Alternatively, the volume-tracking method of Hirt and Nichols[5] and Liang[6] depends on the ability to advect the volume fraction percentage of a computational cell occupied by the liquid through the grid accurately without smearing from numerical diffusion.

In this paper, as a first phase of investigation for droplet dynamics, a computational model based on single liquid droplet oscillation and deformation under convective flows is reported. Fluid is assumed to be inviscid in order to focus on the surface tension effects on the droplet deformation dynamics and to compare calculated results with analytical solutions. The adopted numerical method is based on the arbitrary-Lagrangian-Eulerian (ALE) technique[7] for the solution of time-dependent, two-dimensional, incompressible fluid flows involving a condensed phase dispersed within a gas phase in which the surface tension and/or material interface are presented. The Lagrangian surface tracking scheme and the interface discontinuity (inviscid free-slip material surface) scheme have been specifically developed for this investigation.

Model Description

The model considers the flow of two different incompressible fluids separated by a material interface. The governing

Presented as Paper 90-2309 at the AIAA/SAE/ASME/ASEE 26th Joint Propulsion Conference, Orlando, FL, July 16-18, 1990; received Aug. 13, 1990; revision received July 29, 1991; accepted for publication Aug. 1, 1991.

*Graduate Research Assistant. Student Member AIAA.
†Assistant Professor, Mechanical and Aerospace Engineering. Member AIAA.

equations considering incompressible, inviscid flows for each fluid are

$$\nabla \cdot \boldsymbol{u} = 0$$
$$\rho \frac{\partial \boldsymbol{u}}{\partial t} + \rho(\boldsymbol{u} \cdot \nabla)\boldsymbol{u} = -\nabla P \tag{1}$$

where $\boldsymbol{u}$ is the fluid velocity, P the pressure, and ρ the density. The finite difference scheme adopted in this study is based on the ALE method. The finite difference mesh is a network of quadrilateral cells as shown in Fig. 1. Fluid variables such as pressure, density, and cell mass are defined at the cell centers. Velocity components are defined at cell vertices. The physical interface boundary between two fluids coincides with the cell boundary as shown in Fig. 2. The material interface requires special arrangement when a discontinuity is present. In this case, the interface can be represented by two lines each belonging to the fluid adjacent to it. The special treatment of the interface boundary conditions is presented later.

A detailed description of the ALE numerical method can be found in Ref. 7. Only a brief discussion of this scheme follows. The ALE scheme divides the computations into two stages. In the first stage, the Lagrangian calculations, the computational grid vertices move with the same velocity of the fluid. There is no mass interchange among the computational cells. A predictor-corrector numerical scheme is used to solve the continuity and momentum equations. The predictor first calculates the temporary velocity increment ΔV_{ij}^* for vertex (i,j) at each time step based on a temporary new pressure field P^*,

$$\Delta V_{ij}^* = \frac{\Delta t}{m_{ij}} \oint_s P^* \mathrm{d}A \tag{2}$$

where s is the surface of the momentum control volume, $m_{i,j}$ the vertex mass for point (i,j), and Δt the time increment. Then the positions of vertices are updated as

$$V_{ij}^* = V_{ij}^N + \Delta V_{ij}^*$$
$$X_{ij}^* = X_{ij} + V_{ij}^* \Delta t \tag{3}$$

and the cell mass m_{ij}^* can be calculated based on the temporary volume. If the updated cell mass m_{ij}^* does not agree with the cell mass m_{ij} of the previous time step, the corrector step uses the conjugate-gradient method to find a new pressure field. If the cell mass converges, the velocity and pressure at time $(t + \Delta t)$ can be obtained. Since first stage calculations are pure Lagrangian descriptions, the adoption of this method for complex flows may generate a highly distorted grid system. To cure this difficulty, a second stage rezone calculation is used. In this stage, a new desired grid system is implemented, and a donor-acceptor method is used to calculate the mass and momentum flux change between the Lagrangian cell positions and $(N + 1)$ time step cell positions. The velocity at the $(N + 1)$ time step is then derived at the new grid vertices.

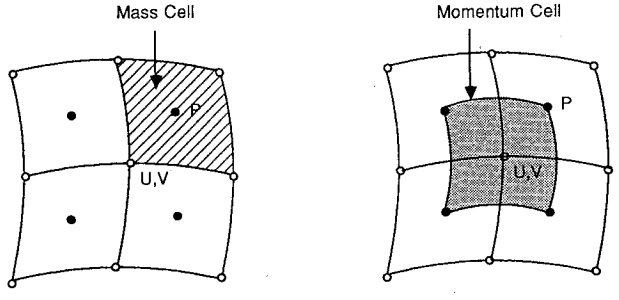

Fig. 1 General grid setup: regular mass and momentum control volume.

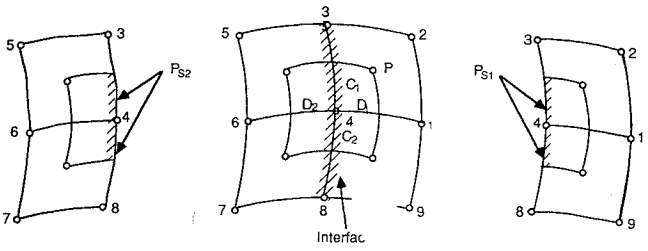

Fig. 2 Interface momentum control volume and surface pressure: points 3, 4, and 8 are interface vertices; P_{s1} and P_{s2} are gas and liquid phase surface pressures respectively.

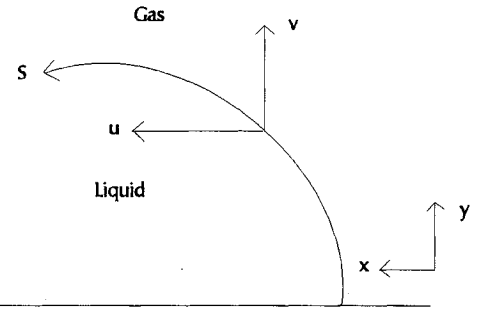

Fig. 3 Droplet surface profile used in calculation of two principle radii of curvature.

Free Surface Treatment

The boundary conditions at the interface between two fluids, under the inviscid (freeslip) assumptions, are equality of the normal velocity component and a pressure jump by surface tension across the interface. The equations can be written as

$$P_i - P_o = \sigma\left(\frac{1}{R_1} + \frac{1}{R_2}\right)$$
$$u_{n1} = u_{n2} \tag{4}$$

where P_i and P_o are the pressure just inside and outside of the interface, respectively, σ is the surface tension associated with the two fluids that define the interface, R_1 and R_2 are the local principal radii of curvature, and u_{n1} and u_{n2} are normal particle velocity components just inside and outside of the droplet surface.

The surface tension force at an interface between two fluids depends on the curvature of the interface, as described in Eqs. (4). For an arbitrarily shaped surface, the principal radii of curvature are very difficult to find both theoretically and numerically. But in the present work, we deal with the two-dimensional or axisymmetric surface. In this case, these principal radii of curvature can be specified relatively simply. Let the drop profile be a parametric form of $y = y(s)$, $x = x(s)$, where y is the distance from axis of symmetry, x is another distance along the axis, and s is the distance along the material interface, shown in Fig. 3, then the radii of curvature for the axisymmetric surface can be obtained as

$$\frac{1}{R_1} = \frac{x'y'' - y'x''}{(x'^2 + y'^2)^{1.5}}$$
$$\frac{1}{R_2} = \frac{x'}{y(x'^2 + y'^2)^{0.5}} \tag{5}$$

where x', y', x'', and y'' are derivatives with respect to the pseudoarc length s. For a two-dimensional surface such as a cylinder, one of the principal radii R_2 is infinity. In this paper, the radius of curvature is calculated from a cubic spline inter-

polation and the sign of the radius depends on whether the surface is concave or convex.

The accuracy of the numerical simulation depends on the implementation accuracy of interface momentum jump conditions that are simplified to the jump conditions as given in Eqs. (4). Various numerical schemes have been developed in order to treat the surface tension force effects on interface momentum flux, or more specific, the interface vertex pressure acceleration calculations. Conventional numerical schemes for surface tension force on interface particle velocity calculations use a finite difference form by fitting vertices on the material interface to some parametric function. This function is then used to find an estimate of local curvatures. Once the curvature is known, a surface tension force is evaluated and used to accelerate the interface vertices. This scheme has the disadvantage that it cannot distinguish the velocity discontinuity, and the calculated pressure conditions across the interface may not satisfy the surface tension jump. Also, since the pressure gradient force and surface tension force are not calculated in the same manner, numerical errors may occur that grow with each time step.

In this paper, as shown in Figs. 2, surface pressure at both sides of the interface is introduced. The surface pressure is defined at a cell surface that coincides with the interface boundary, and the physical pressure drop across the interface is exactly canceled by the surface tension force. The interface is defined by the cell boundaries 84 and 43, where the indexes 8, 4, 3 define interface vertices. P_{s1} and P_{s2} are the surface pressures defined for the interface vertex 4 both inside and outside of the droplet. The surface pressure is assumed to be a constant along the dashed surface. The pressure acceleration uses this surface pressure to integrate Eq. (2) based on the control volume shown in Figs. 2 and to obtain the new surface vertex velocity both inside and outside of the droplet surface. To obtain the surface pressure at each time step during pressure iteration, the normal velocity equality condition in Eqs. (4) has been used. The derivation of the surface pressure is as follows.

For an inviscid fluid contract discontinuity surface, the slip velocity may exist across the interface. Let the slip distance at one time step of the Lagrangian calculation be Δs between points 1 and 2, as shown in Figs. 4. Then from the normal velocity at each vertex,

$$(u_1^{n+1} - u_3^{n+1})\,dy - (v_1^{n+1} - v_3^{n+1})\,dx = 0 \tag{6}$$

where u and v are velocity components in the x and y directions. Velocity components at point 3 can be represented by a neighboring point velocity through the first-order approximation

$$u_3^{n+1} = u_1^{n+1} + \Delta S^{n+1}\left(\frac{\partial u}{\partial S}\right)$$
$$v_3^{n+1} = v_1^{n+1} + \Delta S^{n+1}\left(\frac{\partial v}{\partial S}\right) \tag{7}$$

The pressure acceleration on each side of the vertices can be calculated using a one-sided difference that includes the surface pressure P_{s1} and P_{s2}

$$\Delta V_{ij}^{n+1} = V_{ij}^{n} + \frac{\Delta t}{m_{ij}} \oint_s P^{n+1}\,dA \tag{8}$$

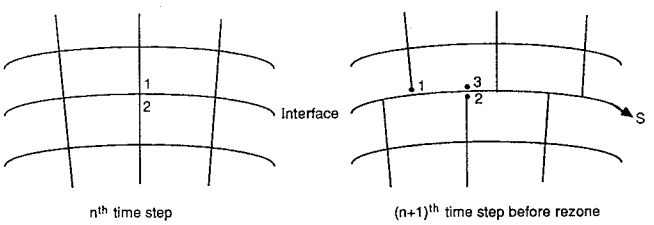

Fig. 4 Interface slip conditions.

and a surface pressure jump according to Eqs. (4) is considered when Eq. (8) is integrated. By substituting Eqs. (7) and (8) into the normal velocity constraint, Eq. (6), a surface pressure formulation can be obtained.

Surface Tracking and Grid Reconstruction

A fully Lagrangian method seems to be the most natural way to track the interface accurately because of vanishing numerical diffusion, but the implementation of Lagrangian tracking encounters two difficulties. One is associated with vertex accumulations along one part of the surface leaving another part with insufficient grid resolution. The other is associated with severe grid distortion or crossing in complex flows. It is well known that, when the governing equations are approximated on a highly distorted grid, the solution loses accuracy. To maintain the benefit of Lagrangian tracking while avoiding its associated shortcomings, a combined Lagrangian and regriding method is used in the current study. The positions of the free moving interface vertices are tracked by a purely Lagrangian method in order to get accurate surface development; that is, no mass flux across the interface. Because of the the discontinuity across the interface, the vertex position and velocity on both sides close to the interface were tracked. As a result, the droplet surface is represented by the inner surface vertex positions. To maintain good interface resolution as the droplet deforms, a higher-order cubic spline interpolation method has been used at each time step to generate a uniform vertex distribution along the Lagrangian surface. Also, the corresponding vertex velocity at each new position is calculated from the cubic spline interpolations for both sides near the interface. These velocity were then used to calculate the mass and momentum convective flux inside and outside of the droplet surface. The momentum average velocity on the interface momentum control volume gives initial conditions for the next time step interface vertex Lagrangian velocity. Once the surface vertex positions are determined at the new time step, grid reconstruction is performed. The most efficient way to avoid grid crossing is to keep the grid lines as orthogonal as possible. It is logical to take the coordinates to be solutions of a system of partial differential equations with Dirichlet boundary conditions.[8] In general, these considerations lead to a grid generator based on Poisson-type equations. By choosing the right-hand-side control functions of the Poisson equations, we control the contraction of the grid lines. Currently, a Poisson solver with weak constraints on the forcing functions, which is similar to the constraint function developed in Ref. 9, is employed to regenerate the grid for those vertices not on the interface at each time step in the rezone phase.

Results

Droplet Oscillation

The nature of vibrations of a liquid drop about a spheroidal shape was first investigated by Rayleigh.[10] Using the potential flow assumptions, Rayleigh was able to derive the frequency of oscillation as

$$\omega_n^2 = (n^3 - n)\frac{\sigma}{(\rho_d + \rho_e)R^3} \tag{9}$$

where ρ_d and ρ_e are the droplet and external fluid density, respectively, R is the radius of undisturbed cylindrical jet, and σ the surface tension coefficient. The values $n = 0$ and $n = 1$ correspond only to rigid-body motion. The fundamental mode is $n = 2$, and the amplitude of oscillation of a cylindrical jet at any instant is given in polar coordinates as

$$r = a + \epsilon \cos(n\theta) \tag{10}$$

where ϵ is the small disturbance amplitude and a is the radius of the undisturbed cylindrical jet.

To test the surface tension algorithm, a series of calculations on droplet oscillations in a normal mode have been conducted, and results for three different sets of density ratio conditions will be discussed.

The initial droplet geometry was chosen as

$$a = 0.01 \text{ cm}$$

$$\sigma = 15 \text{ dyne/cm} \tag{11}$$

$$\epsilon = 0.05a$$

The droplet radius a is chosen to be a typical sized droplet in a real combustor. The surface tension coefficient σ is chosen arbitrarily in the current studies and it can be defined based on real physical properties. The three different test conditions and results are shown in Table 1. Figures 5 show the position as a function of time of the right most vertex of the droplet compared with the theoretical curve from Rayleigh's theory. For density ratios (droplet to external fluid) of 1:1000 and 1000:1, the calculated oscillation periods agree excellently with Rayleigh's analysis; however about 4% difference exists for a density ratio of 2:1 (447:223.5). This is because Rayleigh's original theory considered the unbounded exterior flow, and a

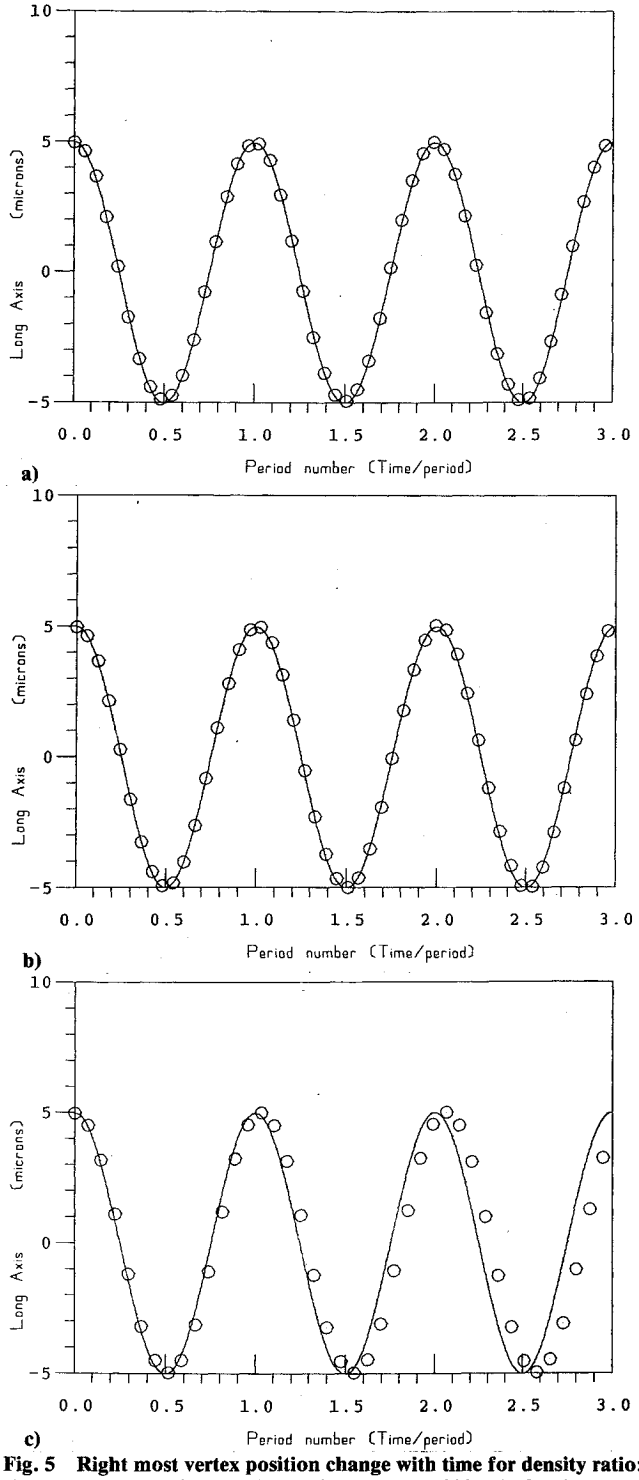

Fig. 5 Right most vertex position change with time for density ratio: a) density ratio 1000:1; b) density ratio 1:1000; c) density ratio 447:223.5.

Table 1 Test results on droplet oscillation

Density ratio, kg/m^3	Theoretical period, s	Calculated period, s
1000:1	6.626E-04	6.626E-04
1:1000	6.626E-04	6.626E-04
447:223.5	5.423E-04	5.560E-04

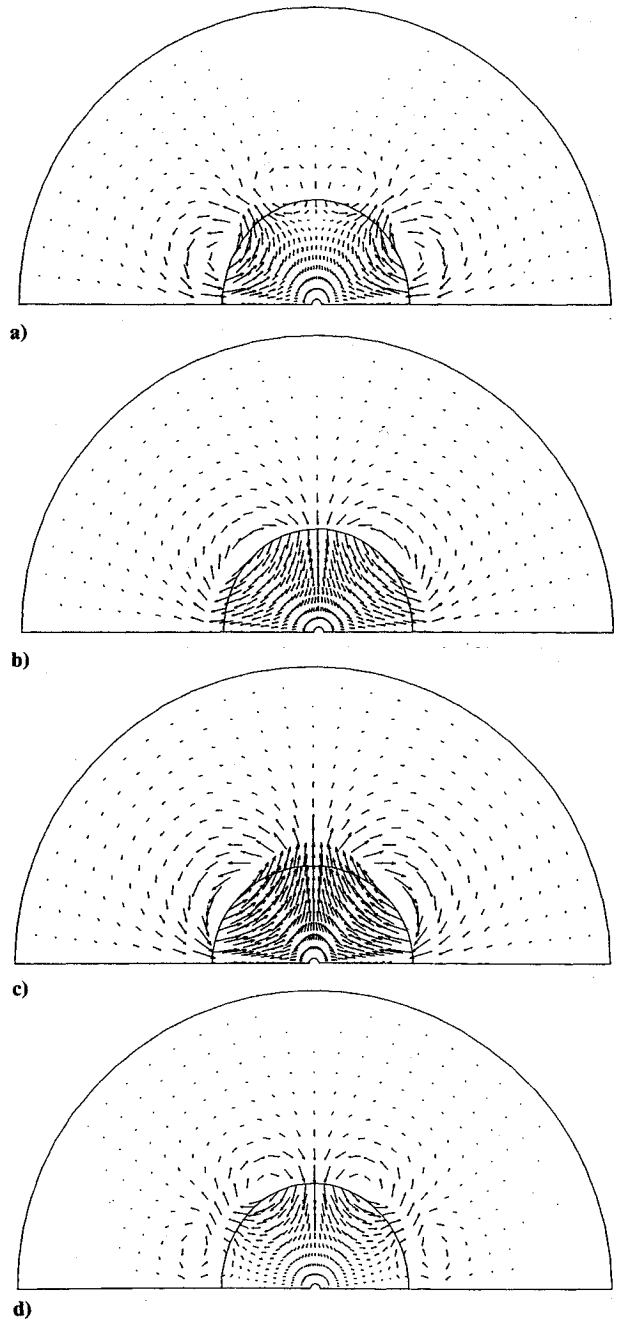

Fig. 6 Velocity distribution at different time steps: a) $T = 0.502$; b) $T = 0.604$; c) $T = 1.207$; d) $T = 1.509$.

finite domain was used in the computation. It is believed that the finite computational domain used in this calculation was the major cause of the difference in the oscillation period for flows with a 2:1 density ratio.

It is also noted that the oscillation amplitude will not decay with time and the oscillation period does not change with time, indicating that the numerical diffusion and dissipation is almost zero in the numerical algorithm. Figures 6 show the velocity fields at different time steps. The velocity field is symmetric to the vertical plane containing the center of the droplet, even at the transition time from short axis to long axis, such as at $t=0.502$ and 1.509 periods. This velocity distribution inside the droplet is similar to the experimental photographic results obtained by Trinh et al.[11] for mode 2 small amplitude oscillation.

Droplet Deformation

The competition tendency between the aerodynamic force and the surface-tension force and their effects on droplet deformation can be related to the Weber number, which represents the ratio of external aerodynamic force to the surface-tension force, and the Bond number, which represents the ratio of internal hydrodynamic pressure to surface tension force. To determine the breakup mode, the most common criterion is the critical Weber number, although it is not the only controlling parameter for determining droplet behavior in a gas flow. Basically, three secondary droplet-breakup regimes have been observed.[12,13]

Regime 1:

This regime is a parachute-type (bag-type) breakup and chaotic destruction in which the droplet flattens in the direction perpendicular to the flow and forms a shroud extending along the direction of gas motion. This shroud either breaks off, producing a group of small droplets, or several parachutes are formed from one droplet, which in the final stage produces groups of fine droplets. In this case,

$$8 \le W_e \le 40$$
$$0.2 \le W_e R_e^{-0.5} \le 1.6 \tag{12}$$

Regime 2:

This regime is a stripping-type breakup in which the gas flow tears off shrouds from the flattened droplet followed by the disk-shaped droplet reaching its critical deformation and decomposing into several smaller droplets. In this case,

$$20 \le W_e \le 2.0 \times 10^4$$
$$1.0 \le W_e R_e^{-0.5} \le 20 \tag{13}$$

Regime 3:

This regime is an explosion-type breakup where

$$2.0 \times 10^3 \le W_e \le 2.0 \times 10^5$$
$$20 \le W_e R_e^{-0.5} \le 200 \tag{14}$$

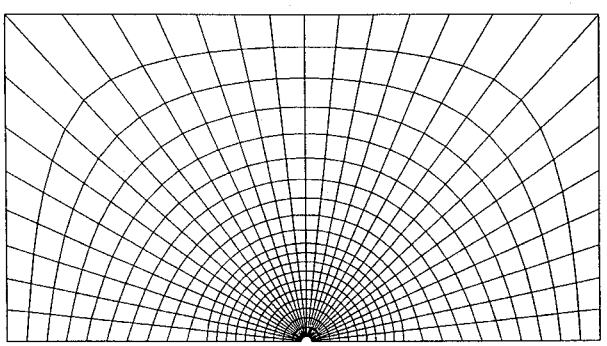

Fig. 7 Initial grid for droplet deformation calculations.

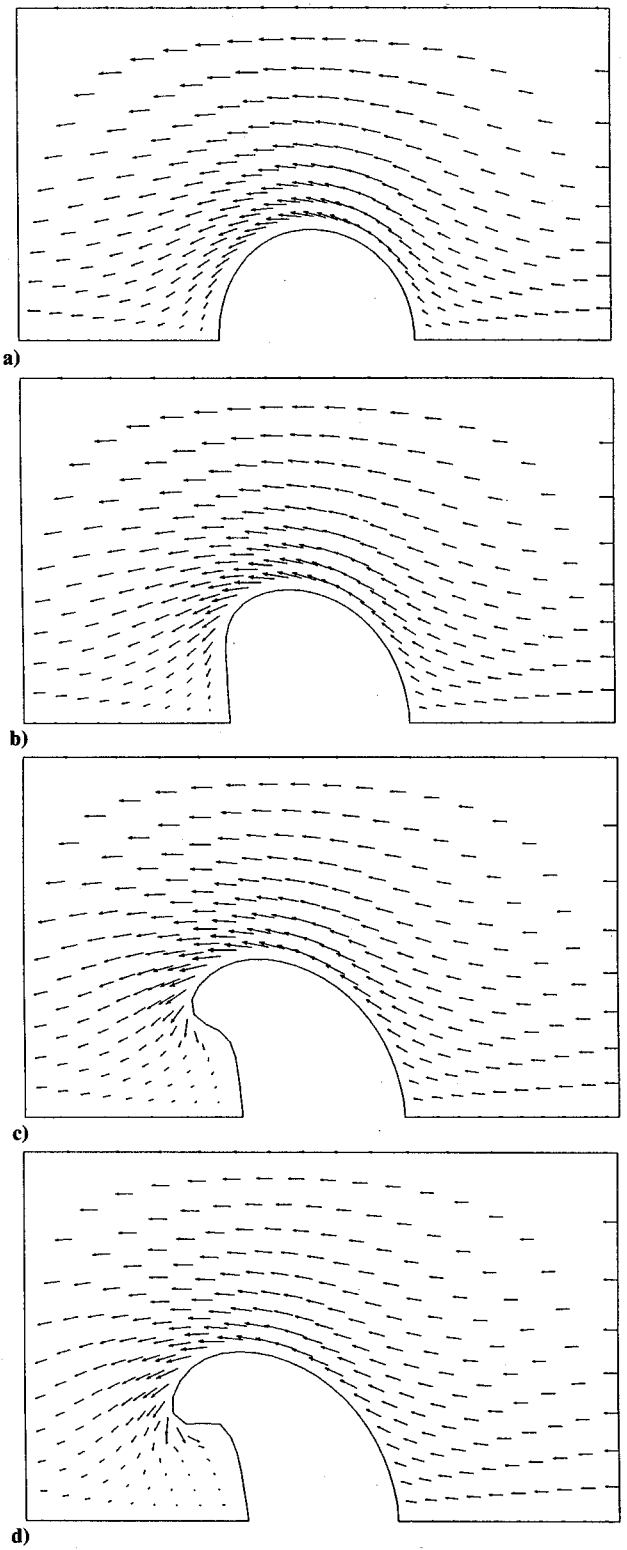

Fig. 8 Velocity distribution and surface shape at different time steps for density ratio 447:223:5: a) $T = 5$ μs; b) $T = 10$ μs; c) $T = 15$ μs; d) $T = 18$ μs.

where W_e and R_e are Weber and Reynolds numbers respectively. The critical Weber number depends on the time variation of the relative velocity between the droplet and the external fluid. Since the breakup process takes a finite amount of time, the length of time for which the flow acts on the droplet may determine whether breakup will actually occur, even though the criteria may be satisfied. It is pointed out by Borisov et al.[13] that the characteristic deformation time (which is the time for droplet deformation to reach a critical stage) is very important in determining the type of breakup.

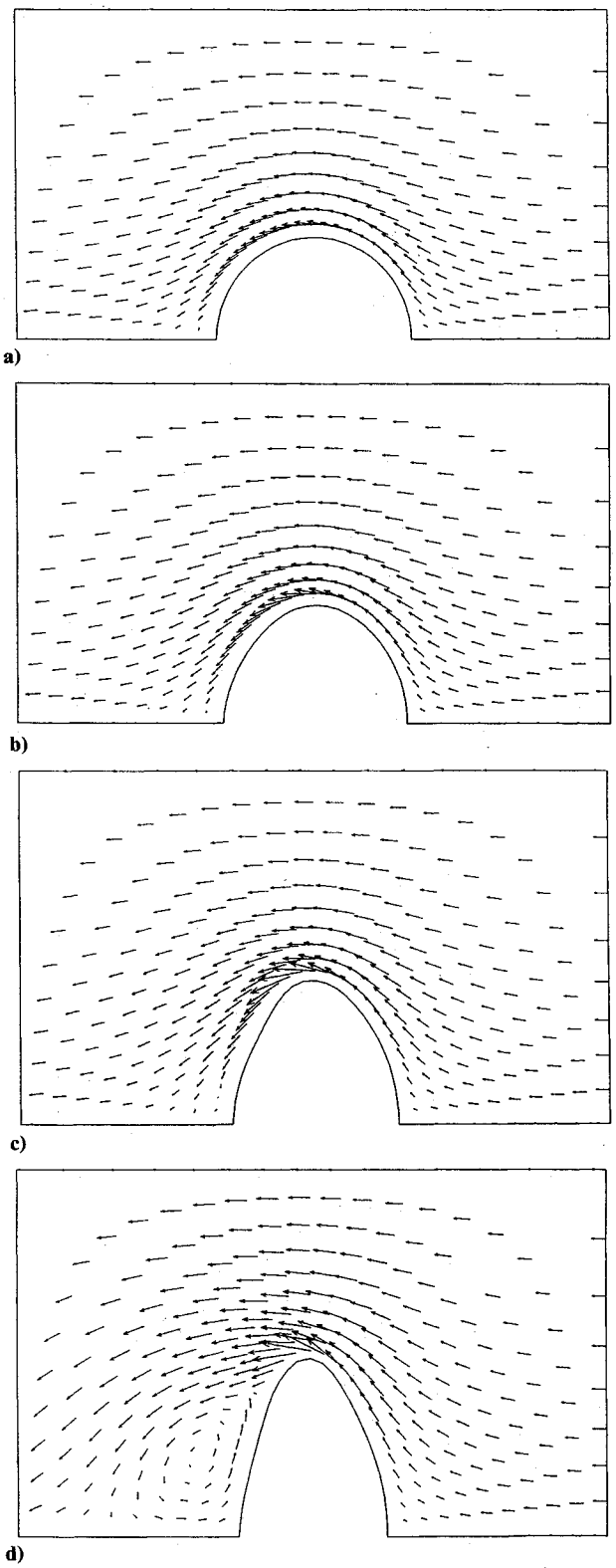

Fig. 9 Velocity distribution and surface shape at different time steps for density ratio 1000:1: a) $T = 50$ μs; b) $T = 110$ μs; c) $T = 160$ μs; d) $T = 210$ μs.

To study droplet deformation in convective flows, a series of calculations have been made. The two-dimensional deformation test case considers incompressible, inviscid flows around an initially stagnant cylindrical droplet. The selected parameters are as follows: droplet density = 447.0 kg/m^3; droplet/external fluid density ratio = 2:1; external fluid density = 223.50 kg/m^3; surface tension $\sigma = 15$ dyne/cm; initial droplet spherical diameter = 200 μ; and inlet relative velocity = 10 m/s.

Figure 7 shows the initial grid setup for the droplet deformation calculations. The initial Weber number based on the initial geometry and relative velocity is 74.5. The Reynolds number for this inviscid flow is infinitely large. As time progresses, the relative velocity between the droplet and the external fluid decreases for sudden acceleration conditions. This process reduces the Weber number, which puts the breakup regime in the parachute mode. Figures 8 show the velocity field and droplet surface evolution at different time steps. After deformation starts due to sudden acceleration, the surface geometry changes, which in turn significantly changes the surface-tension force along the surface. The pressure force competes with the surface-tension force, which drives the flow in the wake of the droplet to establish recirculation. The droplet surface deforms into a parachute-type at 18 μs. At 10 μs, the rear of the droplet surface becomes flattened, and the surface tension force is reduced significantly. Since the restoring force provided by surface tension is relatively small, further deformation instead of oscillation occurs, leading to the trend of bag-type breakup. This result is consistent with the results obtained by Fritts et al.[2]

A test case was also conducted for a density ratio of 1000:1 (droplet density 1000 kg/m^3), where all other parameters were the same as the first case. The initial Weber number is 0.333. Figures 9 show the external flowfield and droplet surface evolution at different times. As time increases, the maximum velocity of the flow increases due to droplet deformation. At 210 μs, the calculated maximum external velocity is 39 m/s and the corresponding Weber number based on this velocity is less than 6.0.

The droplet extends first in the direction normal to the external flow direction, then the edge of the droplet becomes flattened. At 160 μs, the recirculation zone starts to build up. At 210 μs, the recirculation zone is well established.

Comparison with Experimental Results

A spherical droplet deformation/oscillation calculation has been conducted in order to compare to freely falling droplet experimental results. Details of the experimental setup can be found in Ref. 14. A droplet-on-demand injector, based on a design similar to that reported by Switzer[15] at Wright Patterson Air Force Base in Ohio, was used to generate an initially deformed droplet. The droplet shape and its average velocity were determined photographically by a silhouette imaging system. The droplet shape at different stages of deformation is shown in Figs. 10.

The numerical simulation considers a water droplet. A water-air interface surface tension is chosen to be 72.75 dyne/cm. From the experimental measurements, the initial droplet diameter is about 90 μ and the average relative velocity is 3.0 m/s. The initial shape of the droplet was considered to be the mode 3 deformation proposed by Rayleigh. The theoretical linear prediction for the pure droplet oscillation period is 40.62 μs. The experimental measurement shows that the oscillation period is about 52 μs, which differs from the linear theory because of viscous effects and large amplitude oscillations. The numerical prediction of the oscillation period is about 42 μs, which deviates from the theoretical value by 3.40% and underestimates the experimental value. The reasons for this deviation are as follows. The numerical simulation uses the $n = 3$ normal mode initial geometry to start the calculation, as identified at 0 μs in Figs. 10. The experimental velocity distributions both inside and outside of the droplet are unknown and the initial condition for the numerical calculation differs from the experiment. Because of the nonzero initial velocity field, droplet oscillation in the experiment most probably contains other modes of oscillation.

Figures 10 show a comparison of experimental droplet surface and numerical results at various times. General agreement is found for droplet surface shape. The experimental surface evolution is faster than that of the numerical predictions, indicating that the deformation happened very fast and may

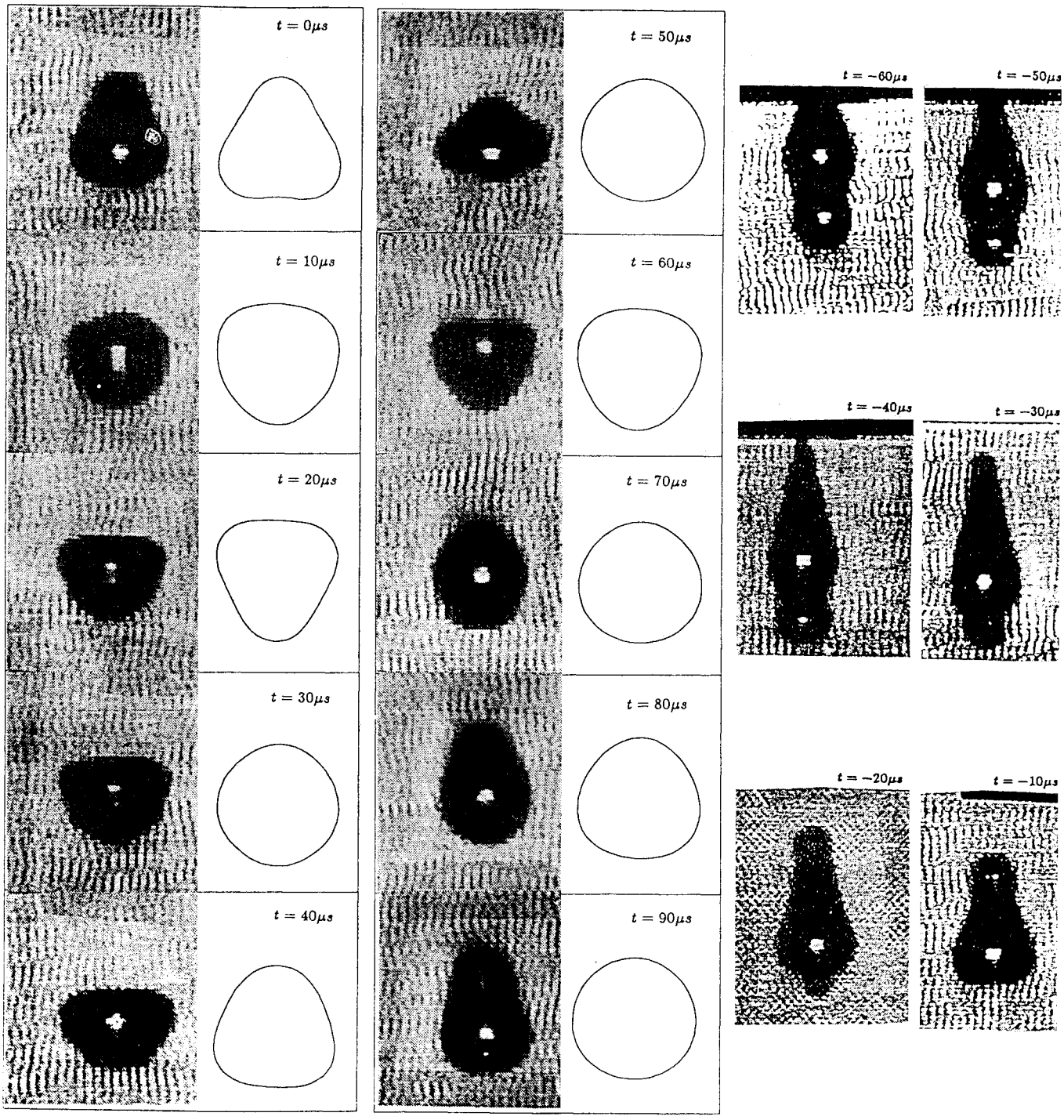

Fig. 10 Droplet surface shape comparison (at $t \leq 0$, no comparison was made).

not be a gradually changing process. Also notice that the numerical simulation results does not include the viscosity, which is a major damping factor in the experiment. The initial Weber number for the experiment is $2.78(10)^{-03}$. In this case, the numerical results show that the characteristic deformation time is comparable to the droplet oscillation time, which is consistent with Ref. 11.

Concluding Remarks

A new interface surface tension technique has been developed and used to calculate droplet deformation and oscillation. The surface pressure formula works well for the interface discontinuity. The numerically predicted droplet oscillation frequency agrees closely with that derived from linear theory. Numerical diffusion and dissipation are almost zero in the adopted scheme. The results of two-dimensional droplet deformation simulation show that the deformation process is consistent with experimental observations. The spherical droplet deformation/oscillation simulation has also been compared to experimental results yielding good agreement.

References

[1]Oran, E. S., and Boris, J. P., *Numerical Simulation of Reactive Flow,* Elsevier, New York, 1987, pp. 358–391.

[2]Fritts, M. J., Fyfe, D. E., and Oran, E. S., "Numerical Simulation of Fuel Droplet Flows Using a Triangular Mesh," NASA CR 168263, 1984.

[3]Fyfe, D. E., Oran, E. S., and Fritts, M. J., "Numerical Simulation of Droplet Oscillation, Breakup, and Distortion," AIAA Paper 87-0539, Jan. 1987.

[4]Fyfe, D. E., Oran, E. S., and Fritts, M. J., "Surface Tension and Viscosity with Lagrangian Hydrodynamics on a Triangular Mesh," *Journal of Computational Physics,* Vol. 76, 1988, pp. 349–384.

[5]Hirt, C. W., and Nichols, B. D., "Volume of Fluid (VOF) Method for the Dynamics of Free Boundaries," *Journal of Computational Physics,* Vol. 39, 1981, pp. 201–225.

[6]Liang, P. Y., Eastes, T. W., and Gharakhari, A., "Computer Simulation of Drop Deformation and Drop Breakup," AIAA Paper 88-3142, July 1988.

[7]Hirt, C. W., Amsden, A. A., and Cook, J. L., "An Arbitrary Lagrangian-Eulerian Computing Method for All Flow Speeds," *Journal of Computational Physics,* Vol. 14, 1974, pp. 227–253.

[8]Thompson, J. F., Warsi, Z. U. A., and Martin, C. W., "Boundary-fitted Coordinate Systems for Numerical Solution of Partial Differential Equations—A Review," *Journal of Computational Physics,* Vol. 47, No. 1, 1982, pp. 1–108.

[9]Warsi, Z. U. Z., "Numerical Generation of Orthogonal and Non-Orthogonal Coordinates in Two Dimensional Simply- and Doubly-Connected Regions," Von Karman Inst. for Fluid Dynamics, TN 151, Brussels, May 1984.

[10]Rayleigh, L., "On the Capillarity Phenomena of Jets," *Proceedings of the Royal Society of London,* Vol. 29, 1879, p. 71.

[11]Trinh, E., Zwern, A., and Wang, T. G., "An Experimental Study of Small-Amplitude Drop Oscillation in Immiscible Liquid System," *Journal of Fluid Mechanics,* Vol. 115, 1982, pp. 453–474.

[12]Fenenberg, A., and Jaqua, V., "Atomization and Mixing Study Interim Report," NASA CR 170943, 1983.

[13]Borisov, A. A., Gel'fand, B. E., Natanzon, M. S., and Kossov, O. M., "Droplet Breakup Regimes and Criteria for Their Existence," *Journal of Engineering Physics,* Vol. 40, No. 1, 1981.

[14]Norton, C. M., "An Experimental Study of Droplet Combustion at High Pressures," M.S. Thesis, Univ. of Tennessee Space Inst., Tullahoma, TN, 1990.

[15]Switzer, G. L., private communication, 1989.